Plasmon enhanced fluorescence of carbon nanodots in gold nanoslit cavities

By: Bhawna Bagra, Wendi Zhang, Zheng Zeng, Taylor Mabe, and Jianjun Wei

B. Bagra, W. Zhang, Z. Zeng, T. Mabe, J. Wei, Plasmon enhanced fluorescence of carbon nanodots in gold nanoslit cavities, *Langmuir*, **2019**, 35, 8903-8909. DOI: 10.1021/acs.langmuir.9b00448.

Abstract:

Carbon nanodots (CNDs) are featured with a wide range of light absorption and excitation-dependent fluorescence. The emission enhancement of CNDs is of great interest for the development of nanophotonics. Although the phenomenon of plasmon-enhanced fluorescence for quantum dots and molecular dyes has been well investigated, rarely has it been reported for CNDs. In this work, a series of plasmonic nanoslit designs were fabricated and utilized for immobilization of CNDs in nanoslits and examination of the best match for plasmonic fluorescence enhancement of CNDs. In concert, to better understand the plasmonic effect on the enhancement, the surface optical field is measured with or without CND immobilization using a hyperspectral imaging system as a comparison, and a semianalytical model is conducted for a quantitative analysis of surface plasmon generation under the plane-wave illumination. Both the fluorescence and surface reflection light intensity enhancement are demonstrated as a function of nanoslit width and are maximized at the 100 nm nanoslit width. The analysis of surface plasmon–exciton coupling of CNDs in the nanoslit area suggests that the enhancement is primarily due to plasmonic light trapping for increased electromagnetic field and plasmon-induced resonance energy transfer. This study suggests that incorporating CNDs in the plasmonic nanoslits may provide a largely enhanced CND-based photoemission system for optical applications.

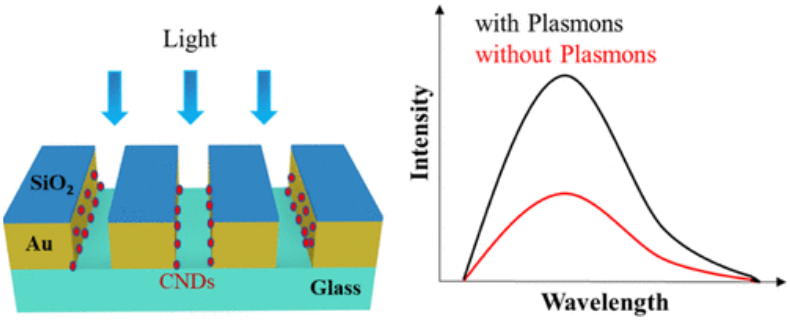

Keywords: Carbon nanodots (CNDs) | plasmonic nanoslits | photonics

Article:

Introduction

Fluorescence is one of the most utilized phenomena in various fields such as optical devices, microscopy imaging, biology, medical research, and diagnosis. For many of these applications, it is desirable to enhance the fluorescence to obtain a greater signal from few samples. Surface plasmons (SPs)[1,2] on subwavelength nanostructured surfaces were found to be capable of fluorescence enhancement.[3] The optical phenomena of SPs lie considerably in the conductive surfaces through manipulating the geometry of subwavelength apertures with a periodic structure.[4,5] The plasmonic-enhanced fluorescence results in a variety of applications, such as biodetection and biosensing schemes.[6,7] Specifically, many cancer biomarkers, hormones, allergens, and proteins have been detected by SP resonance (SPR) biosensors with high accuracy and sensitivity.[8] Nevertheless, improving fluorescence sensitivity for single molecular detection is still undertaken for the development of the next-generation fluorescent systems.[9−12]

Propagating or localized SPs can couple to incident photons, resulting in a confinement of the electromagnetic (EM) field. This interaction is associated with large enhancement of the field and local optical density of states. When a fluorophore is coupled to the plasmonic-coupling surface, the enhanced field can be utilized to increase excitation rate, thus enhancing and controlling far-field angular distribution of fluorescence.[13] Further, because of their high sensitivity to geometry and surroundings, SPs can concentrate light within subwavelength volumes.[14,15] Lately, plasmon coupling interaction has been used to increase light absorption and fluorescence of carbon nanodots (CNDs) based on coupling to a localized SPR (LSPR) of metallic nanoparticles.[16,17]

CNDs have attracted great attention because of their promising characteristics such as strong, tunable photoluminescence and good optoelectronic properties.[18,19] The fluorescence in CNDs is due to band gap transitions, but the nature of the transitions is not fully understood.[20−23] These transitions could arise from conjugated π-domains, bond disorder-induced energy gaps,[24,25] and/or giant red-edge effects that give rise to fluorescence depending on strong excitation wavelength.[26,27] Light emission has also been attributed to quantum confinement effects,[28] size-dependent optical properties,[29] surface-related defect sites,[30] and radiative recombination of excited surface states.[31]

While plasmonic enhancement of fluorescence from quantum dots (QDs) or dye molecules has been investigated,[13,32−34] the research of the plasmonic effect on the fluorescence of CNDs is rare, especially CNDs on nanostructured conductors. Instead, CNDs were reported to have a plasmonic effect to increase the fluorescence of ZnO QDs.[35] Over the past few years, a significant amount of work has been done to enhance the fluorescence of CNDs by working on tuning their structures. It has been noticed recently that fluorescence of CNDs can be enhanced on the gold films when CNDs were labeled on bacteria cells.[36]

Considering that the fluorescence properties of CNDs could be modulated by the enhanced fields derived from the spatially confined SPs corresponding to the optical excitation at or near the resonant energies, there are few findings on the LSPR and/or SP polariton (SPP) effect and how it helps in the enhancement of fluorescence of CNDs. It would also be interesting to find out the fundamental relationship between the fluorescence enhancement and the surface plasmon

generation (SPG) efficiency. Here, the SPG is described as the rate of SPP launching, propagation, and scattering by matching the continuous EM field quantities at the dielectric–metallic interface.[37,38] Recently, we observed the plasmon–exciton coupling effect on light energy conversion to photocurrent by a system where photosystem I is embedded in plasmonic nanoslits and correlation to the SPG efficiency of the nanoslit-based photoelectrochemical cell.[39]

In this study, a nanoslit design for fluorescence enhancement setup is used and fluorescence enhancement of CNDs in these plasmonic nanoslits is observed. The CNDs are immobilized in a nanoscale slit, and the nanoslit is illuminated with a light source for spectral and fluorescent imaging measurements (Figure 1). The nanoslit arrays used in this study have slit widths of 50, 100, 200, 300, 400, or 500 nm. The present work demonstrates that tuning the width of the nanoslit provides a good match for CND excitation and induces fluorescence enhancement from the CNDs immobilized in nanoslit arrays. The fluorescence enhancement correlates to the nanoslit width-dependent SPG efficiencies. In concert, the near-field light intensity spectra are measured in a reflection mode upon an incident white light as a comparison to the fluorescence enhancement. The mechanisms for the optical enhancement are discussed on the basis of plasmonic–exciton coupling interaction in the nanoslit gap.

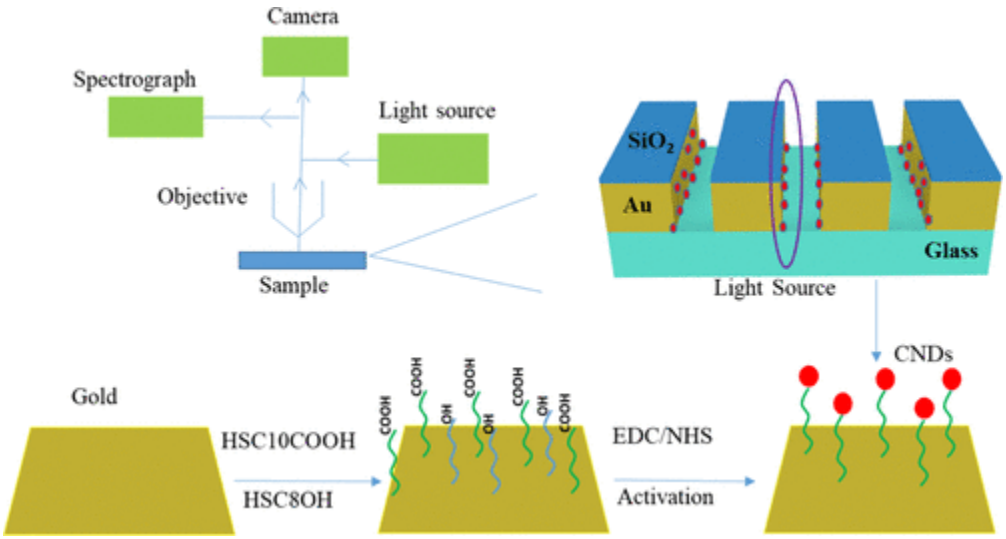

Figure 1. Schematic view of the setup used for the light intensity measurements (top) and illustration of the protocol for the SAM formation and CND immobilization on the gold nanoslit surfaces (bottom).

Experimental Section

Synthesis and Characterization of CNDs. CNDs were synthesized from urea and citric acid using a previously reported microwave-assisted procedure.[19,40] Briefly, citric acid (1.0 g, 99%, Acros Organics) and urea (1.0 g, 99.5%, Aldrich) were simultaneously added to 1.0 mL of deionized (DI) water forming a homogeneous solution. Then, a microwave synthesizer (CEM Corp 908005) was used to heat the solution (300 W for 18 min). Next, to remove aggregated and large particles, the cold aqueous reaction solution was purified using a centrifuge (Sorvall Legend XFR floor model centrifuge) for 20 min at 3500 rpm. The sample was dialyzed for 24 h

(1000 molecular weight cutoff, Fisher Scientific) against DI water (three times) to purify the dark-brown solution. Last, a freeze-dryer (FreeZone 6, Labconco) was used to dry the resultant solution for 24 h to obtain the solid sample.

Atomic force microscopy (AFM, 5600LS AFM, Agilent) was used to test the size of the purified CNDs on a freshly cleaved mica surface. To study the chemical structure and elemental content of the CNDs, Fourier transform infrared spectroscopy (FTIR, 670 FTIR, Varian) was used. UV–vis spectroscopy (Cary 6000i, Agilent) and fluorescence spectroscopy (Cary Eclipse, Agilent) were used to study the optical properties of the CNDs. Both UV–vis and fluorescence were obtained using CNDs dissolved in DI water at a concentration of 0.05 mg/mL.

Fabrication of the Device. Glass cover slips were used as substrates and were cleaned in a piranha bath (3:1 H_2SO_4/H_2O_2), rinsed with DI water, dried with a nitrogen stream, and cleaned in an oxygen plasma (200 W, 2 min). The substrates were then dehydrated on a hot plate at 180 °C. Metal deposition was performed by e-beam evaporation (Kurt Lesker PVD75 e-beam evaporator). After reaching a base pressure of 1.4×10^{-6} Torr, Ti was evaporated at a rate of 0.3 Å/s to a thickness of 2.2 nm, Au was evaporated at a rate of 1.2 Å/s to a thickness of 150.3 nm, and then Ti was evaporated at a rate of 0.4 Å/s to a thickness of 2.4 nm. SiO_2 was used as a capping layer, and 10.2 nm was deposited atop the final Ti layer at a rate of 0.8 Å/s. Nanoslits were milled in the center of each substrate with focused ion beam milling using a 30 kV, 50 pA probe and a dose of 0.250–0.400 nC/μm^2 (Zeiss Auriga). Each device was milled to have either one slit (with slit widths of 50, 100, 200, 300, 400, or 500 nm) at the center (Figure S1) or an array of nanoslits of different widths (50, 100, 200, 300, or 400 nm) with a periodicity of 500 nm (Figure S2). As a control, a burn box was made by completely milling an area the same size as the nanoslit arrays.

Preparation of Immobilized CNDs onto the Gold Surface. Gold-coated cover slips with individual or arrayed nanoslits were first cleaned with O_2 plasma (South Bay Technologies PC2000 Plasma Cleaner) for 10 min. The coverslips were then incubated in a mixture of 11-mercaptoundecanoic acid ($HS(CH_2)_{10}COOH$, Sigma-Aldrich) and 8-mercapto-octanol ($HS(CH_2)_8OH$, Sigma-Aldrich) in an absolute ethanol solution (Acros Organics) with a 1:2 mole ratio for 24 h to form a self-assembled monolayer (SAM). After SAM formation, the gold slides were incubated in 0.5 mM 1-(3-dimethylaminopropyl)-3-ethylcarbodiimide hydrochloride (TCI)/*N*-hydroxysuccinimide (Sigma-Aldrich) for 2 h to activate the carboxylic acid groups. Next, the gold slide was rinsed with DI water and immediately moved to a freshly prepared 10 mL solution containing 0.05 mg/mL of CNDs for 2 h. The gold cover slips were rinsed with DI water and dried before the experiment.

Fluorescence Imaging and Intensity. Fluorescence measurements were carried out using an Axio Z2M microscope in reflection mode. Axio Z2M microscope is an optical microscope with different filters (blue, green, red). For fluorescence measurements in reflection mode, images were acquired using a 20× objective lens, 9.25 s exposure time, and one of two filters: 430 nm (395–440 nm) or 480 nm (450–490 nm). These fluorescent images of the nanoslits were converted into gray-scale images by MATLAB program, and then ImageJ software was used to calculate the fluorescence intensity.

Reflection Intensity Measurement. In addition to the Axio Z2M microscope, intensity measurements were also carried out using hyperspectral imaging (CytoViva). The CytoViva hyperspectral imaging system has both an optical imaging mode and a hyperspectral imaging mode. Hyperspectral imaging technology is specifically developed for spectral characterization and spectral mapping of nanoscale samples. The optical imaging system equipped with a 100× objective lens and white light source (400–1000 nm) was used to focus the sample, allowing the hyperspectral image to be taken. Three measurements were taken for each device before the deposition of CNDs and nine measurements for each device after the deposition of nanodots.

Results

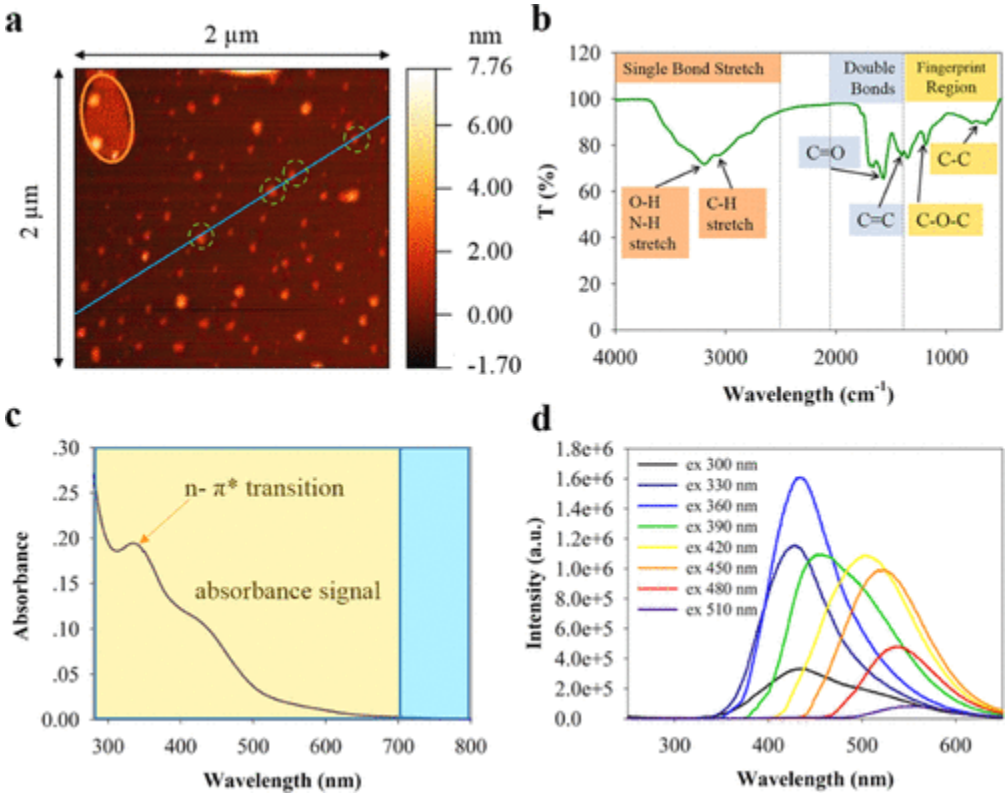

Figure 2. Characterization of the CNDs by different techniques: (a) AFM topography image, (b) FTIR spectra, (c) UV–vis absorption spectra, and (d) fluorescence emission spectra.

CND Synthesis and Characterization. AFM (Figure 2a) with associated height profile analysis (Figure S1) indicates that the CNDs have an average size of about 2–3 nm. Note that some of them are as large as about 5 nm as shown by the orange circle. As a note, because the radius of curvature for the AFM probe is larger than that for the CNDs, the *x* and *y* data do not accurately represent the size of the particles; however, the height data can be used to accurately determine the particle size. According to the FTIR spectra (Figure 2b), ν(N–H) and ν(O–H) are observed according to the presence of broad bands (from 3100 to 3400 cm^{-1}), which suggests that the CNDs are hydrophilic and stable in aqueous solution.[19] The FTIR signals at 765 (C–C), 1182 (C–O), 1418 (C═C), and 1563 (C═O) cm^{-1} are assigned, respectively.[40,41] UV–vis absorption (Figure 2c) shows two main features; the n−π* transition of the C═O moieties can be detected at about 330 nm,[20] and the feature between 400 and 500 nm is attributed to the transition of

surface states.[42] No absorption features can be found above 700 nm. CNDs have been used as a fluorescent dye in bioimaging applications because of their excitation-dependent photoluminescence.[43] Figure 2d shows the fluorescence emission spectra of CNDs in DI water (0.05 mg/mL) under different excitation conditions (λ_{ex} ranging from 330 to 510 nm). The longer excitation wavelength induced an obvious red shift in the fluorescence emission spectra. At an excitation wavelength of 360 nm, a maximum peak emission is observed at 435 nm. Hence, the CNDs are characterized with a diameter of ~2–3 nm sphere, possess surface functionalities (e.g., carboxylates and amines/amides), and display absorbance signals below 700 nm and excitation-dependent fluorescence properties.

Metallic Nanoslit Fabrication and CND Immobilization. Metallic nanoslit films of Au were designed and fabricated to conduct the fluorescence and light illumination experiments. Representative scanning electron microscopy (SEM) images of the nanoslit arrays at slit widths of 50, 100, 200, 300, and 400 nm and individual nanoslits are shown in Figures S2 and S3. The SEM images clearly show straight nanoslits or nanoslit arrays in metallic films. To study the fluorescence and light intensity signals, CNDs were immobilized on both sides of the nanoslit area with a SAM formation using 11-mercaptodecanoic acid and 8-mercapto-octanol.[19] The SAM bridge makes the distance between the CNDs and gold surfaces around 1 nm.

Fluorescence Imaging and Intensity. Fluorescence measurements were taken using an Axio Z2M microscope. The slit arrays of different widths (Figure S2) were used in this measurement because a single nanoslit was invisible under the Axio Z2M microscope. CNDs were immobilized in nanoslit arrays and burn box (control) with a self-assembly method. Figure 3a,b shows the optical fluorescence images and gray-scale images of different width nanoslit arrays under the two excitation wavelengths after deposition of CNDs. There was no fluorescence in the nanoslit array before the deposition of CNDs, but after the deposition of CNDs, strong fluorescence images of the nanoslit arrays were obtained. No or little fluorescence was observed inside the burn box.

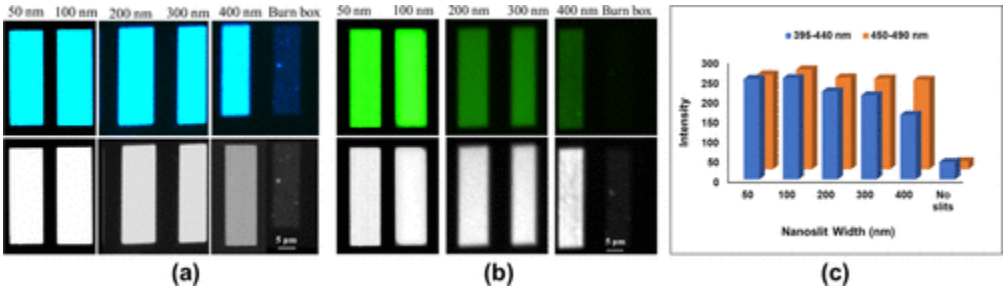

Figure 3. Fluorescence images of different width nanoslit arrays with the Axio Z2M microscope. (a) Upper panel shows the images taken using a 395–440 nm filter light source, and lower panel shows the same fluorescent images when converted to gray-scale images; (b) fluorescence images (upper panel) taken using a 450–490 nm filter and converted gray-scale images (lower panel); and (c) graphic plot showing the fluorescence intensity measured with different filters corresponding to different nanoslit width arrays.

The fluorescence images were converted to gray scale using the MATLAB image processing tool without changing the original intensity. Then ImageJ software was used to calculate the integrated intensity of each nanoslit array using the same area. Figure 3c shows the calculated

intensity of the two different filters used for fluorescent imaging (Tables S1 and S2). The resulting intensity distribution of the nanoslit arrays is similar upon two different excitation lights but slightly higher when using longer excitation wavelength. Regardless of the excitation wavelength, the maximum intensity is observed for the 100 nm width nanoslit array and minimum for the burn box.

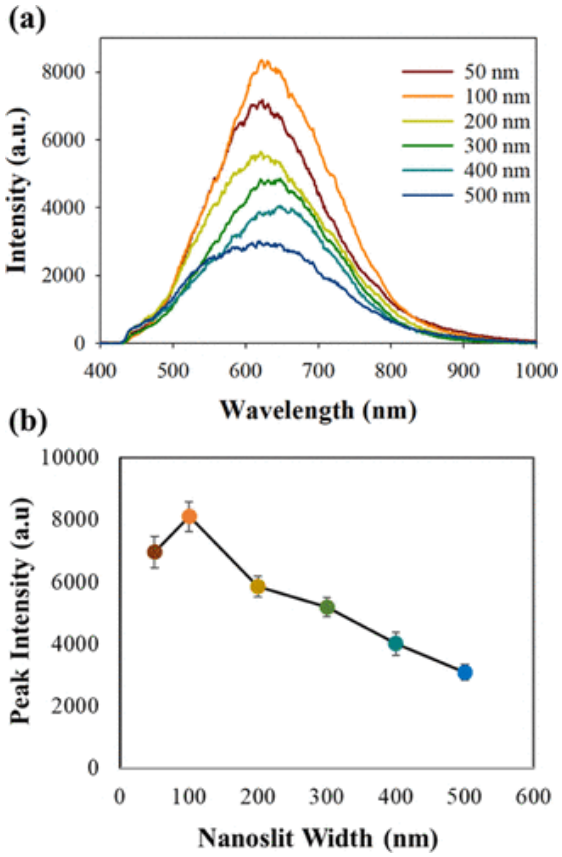

Figure 4. (a) Representative net light intensity spectra of CNDs at different nanoslits after subtracting the light intensity of nanoslits before deposition of CNDs; (b) net peak light intensity for different nanoslits with immobilized CNDs plotted as a function of nanoslit width.

Reflection Light Intensity and Spectra. The reflective light intensity spectra of the immobilized CNDs were obtained by the CytoViva hyperspectral microscope in a reflection mode (Figures S4 and S5). Figure 4a shows representative net intensity spectra measured for different nanoslits after the deposition of CNDs by subtracting the background intensity of nanoslits only. Figure 4b presents the averaged peak intensity of the net light intensity spectra as a function of the nanoslit width (for data, see Tables S3 and S4). Note that the average value of the net light intensity was obtained from nine measurements (three measurements from three devices) for each nanoslit width. The highest light intensity both with and without CNDs was observed when using 100 nm width slits, and this device also presented the highest net intensity. In contrast, the reflective intensity of burned box is very small and insignificant, and the peak intensity is less than 500 a.u. for CNDs on the plane gold substrate versus ~10 000 a.u. in a 100 nm nanoslit. The intensity increases indicate the near-field EM field enhancement by the plasmonic nanoslits. The results from this experiment and the fluorescence show similar trends

with respect to the nanoslit width, suggesting a strong plasmon–exciton coupling effect on the EM field enhancement, which promotes the fluorescence enhancement of CNDs.

SPR Analysis of Gold Nanoslits. To investigate the effect of plasmon–exciton coupling on the fluorescence enhancement, the SPR of various metallic nanoslit structures with respect to the light source was examined. A mechanistic description of the SPP scattering coefficients and efficiencies at the slit apertures is needed regarding the geometric diffraction with the bounded SPP modes launching on the flat interfaces surrounding the slits.[37,38,44,45] The scheme in Figure S7a shows the various parameters of the nanoslit structure to calculate SPG efficiencies "*e*" by a plane wave at normal incidence. The SPG efficiency at one side of nanoslit aperture is calculated according to a semianalytical mode reported earlier.[38,39] The results of SPG analysis are shown in Figure S7b and Tables S5 and S6, which are used in the following discussion for comparison with the experimental results (Figure 5). The SP excitation is efficient at visible frequencies, while "*e*" decreases rapidly with an increase in wavelength. The "*e*" value from a 100 nm nanoslit is the highest when the wavelength of incident light is longer than 600 nm; however, the decreasing nanoslit width increases the "*e*" value with incident light below 600 nm.

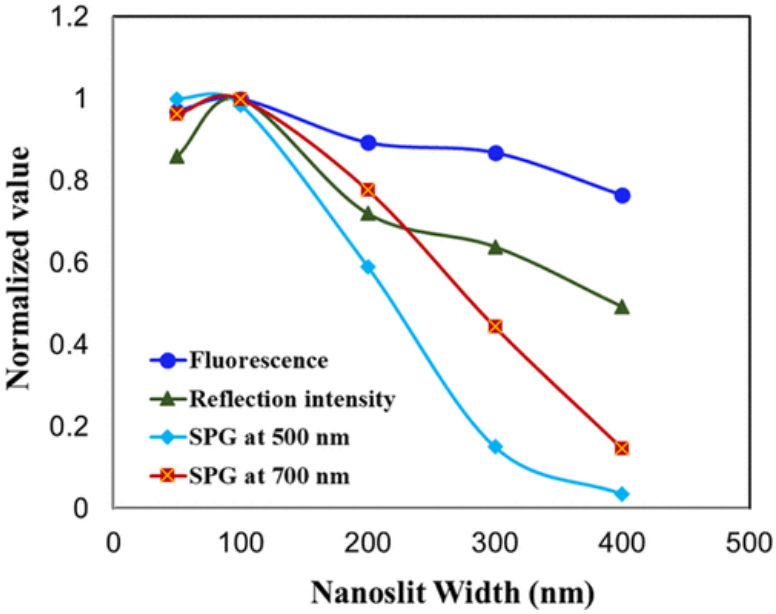

Figure 5. Plot of normalized values of fluorescence and reflection light intensity of CNDs deposited in nanoslits and the SPG efficiencies "*e*" at 500 and 700 nm incident light vs the width of nanoslits.

Discussion

Surface-attached molecular fluorescence signal enhancement depends on the local EM intensity to the molecules, quantum yield, and the energy-transfer process.[6,46−48] Assuming the same quantum yield of CND fluorescence at gold surfaces in different slits, the fluorescence enhancement of CNDs arises from the local EM field enhancement and/or energy transfer. Because the nanoslit structure generates both LSPR and SPP, SP-induced trapping/scattering of incident light in nanoslit cavities containing CNDs will lead to an exciton–plasmon coupling effect, dominating the enhancement of the fluorescence.[47] Hence, a mechanism is required for

SP-coupled emission enhancement and/or excitation enhancement.[6] Namely, there should be some overlap of the SP-induced EM field with the wavelength of photoemission or absorption of CNDs. The reflection spectra show SP-induced light wavelength ranging from 450 to 900 nm (Figures S4 and 4), which has some overlap with the absorption band of CNDs (Figure 2c) (see Figure S8). The fluorescence by two excitation wavelengths at 395–440 and 450–490 nm produces emission spectra from 400 nm up to 650 nm (Figure 2d), and these spectra overlap with the SP-induced EM field as well. It is interesting to observe that there is more emission overlap at the longer excitation wavelength with the local EM field at the excitation light of 450–490 nm. This may be one of the factors that the longer excitation light (450–490 nm) has higher enhancement especially at a larger nanoslit width than that of excitation light at 395–440 nm.

One concern is that why the fluorescence of the immobilized CNDs would not be quenched by the gold surfaces. While fluorescence of a chromophore can be quenched by closely linked gold nanostructures, the quenched fluorescence can be enhanced by a paired plasmonic noble metal nanostructure if there are plasmon coupling interactions. Recently, Zhu et al. reported that fluorescence of a cyanine probe is quenched by a linked gold nanoparticle, but its fluorescence can be turned on when the immobilized probe is put into the gap region of coupled gold nanoparticles.[49] In this work, the CNDs are immobilized in one side of the nanoslit surface and located in the gap of the nanoslit. It is believed that the plasmon–exciton coupling effect in nanoslits is the origin of the fluorescence enhancement. A further analysis is discussed below.

The SPG efficiency is a good parameter to further examine the relative strength of the plasmon–exciton coupling-induced EM field in the nanoslits of different widths and the effect on fluorescence enhancement. For comparison, Figure 5 presents a plot of normalized values of averaged fluorescence, reflected light peak intensities, and the SPG efficiency "*e*" versus the width of nanoslits. Note that the SPG was analyzed without immobilization of CNDs, representing the SP field strength in the nanoslit cavities. Both the fluorescence and reflection light intensities follow the same order of $L_{100} > L_{50} > L_{200} > L_{300} > L_{400}$ (the subscripted number represents the nanoslit width in nm). In other words, the 100 nm nanoslit provides the strongest local field in terms of the enhancement of fluorescence and reflected light intensity, which is reasonably consistent with the calculated SPG efficiency. This suggests that the fluorescence property of CNDs is strongly influenced by the increase in localized EM field, which results from the excitation of the plasmon resonance near the gold nanoslits. A previous report on EM field modeled using a finite-difference time-domain (FDTD) simulation (Figure S9) demonstrated the same order of EM field strength and surface light intensity measurement.[39]

The difference of the fluorescence enhancement from the reflection light and the SPG efficiencies suggests additional energy-transfer process contributing to the fluorescence enhancement. Other than the aforementioned light trapping, there are a few energy-transfer mechanisms proposed for plasmonic enhancement, including fluorescence resonance energy transfer (FRET),[50] hot electron injection (direct electron transfer), and plasmon-induced resonance energy transfer (PIRET).[51,52] The small distance (<10 nm) and absorption overlap between the CNDs and the gold surface makes plasmonic FRET possible, but efficiency is expected to be low because of Stoke's shift energy transfer from the metal nanoslit structure to the CNDs.[50] Meanwhile, the hot electron injection is minimized because of the interfacial barrier and low efficiency (<1%).[53] Considering the lifetime of plasmon, near-field coherent

PIRET would be an alternative process for the efficient plasmonic energy transfer between the gold film in nanoslits and the attached CNDs, while the plasmon still remains excited.[54]

Figure 6 depicts a schematic illustration of plasmon–exciton coupling effect on fluorescence enhancement of CND immobilized in the metallic nanoslit surface. For this hybrid metal–CND system, the plasmonic light trapping and the PIRET between gold nanoslit and CNDs play major roles in the enhanced fluorescence generation. First, the enhanced field by light concentration in the nanoslit presents an overlap with the absorption and emission spectra of CNDs. Second, because of the existence of multiple interband transition dipoles in the CNDs,[19] first-order dipole–dipole coupling between the plasmon in gold, and resonance dipoles in CNDs (purple color array in Figure 6), a resonance energy transfer from the metal film to the CNDs occurs via the PIRET process.[52] It is expected as well that higher SPG efficiency would provide increased dipole–dipole coupling, thus increasing the energy-transfer rate. Both the light trapping and PIRET enable generation of more energetic electrons in CNDs, causing increased populations in the conduction band (CB) from the valence band (VB). As a result, more electrons at the higher energy levels of CB of the CNDs may lead to enhanced photoemission. Furthermore, increased energetic electron generation in the CB potentially increases the kinetics of relaxation to the VB, resulting in more emission per unit time. In this case, the fluorescence quantum yield increases. The above discussion conforms the effective fluorescence enhancement of the CNDs with the SPG efficiency of the plasmonic setup with nanoslit width dependence and maximized enhancement at the 100 nm slit width in this work.

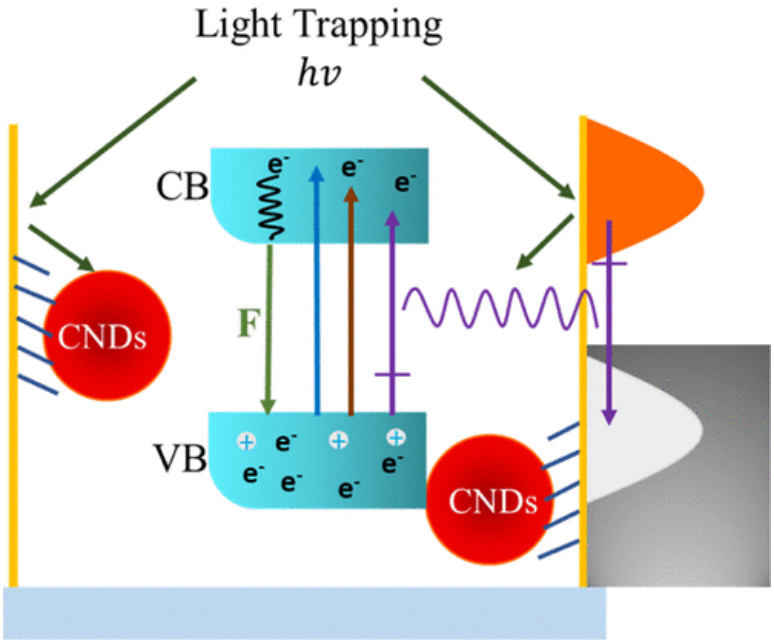

Figure 6. Schematic diagram illustrating the proposed process of fluorescence enhancement of CNDs because of SPR generation and energy transfer in a gold nanoslit.

Conclusions

In this report, we demonstrate the influence of SPR on fluorescence intensity of the CNDs by immobilizing the CNDs on the gold surface in nanoslits. The fluorescence intensity is greatly

enhanced, which corresponds to the calculated SPG efficiency by comparing the experimental results to a semianalytical analysis of the SPG efficiency. Among the studied width of nanoslits at 50, 100, 200, 300, 400, and 500 nm, the 100 nm width nanoslit presents the highest fluorescence enhancement of ∼10× demonstrating an excitation wavelength dependence. The surface optical field measured as a reflection light intensity under a broad-spectrum incident light increases to ∼6× when CNDs are deposited. The results are discussed using the phenomenon of plasmon–exciton coupling focusing on increase in the local EM field surrounding the nanoslit and PIRET. These factors correspond to the enhancement in excitation and modification of emission rate of CNDs that ultimately enhance the fluorescence intensity of CNDs. This study offers promise for the development of a new CND–plasmon-based platform which can be used in optical biosensors and nanoscale optical devices.

Supporting Information

The Supporting Information is available at https://doi.org/10.1021/acs.langmuir.9b00448.

Acknowledgments

This work was performed at the JSNN, a member of South Eastern Nanotechnology Infrastructure Corridor (SENIC) and National Nanotechnology Coordinated Infrastructure (NNCI), which is supported by the National Science Foundation (ECCS-1542174).

This work was partially supported by the US National Science Foundation (NSF) (award#: 1511194), and a North Carolina State fund through the Joint School of Nanoscience and Nanoengineering (JSNN).

The authors declare no competing financial interest.

References

1. Raether, H. *Surface Plasmons on Smooth and Rough Surfaces and on Gratings*; Springer: Berlin, 1988.

2. Hao, Q.; Yang, F.; Yin, Y.; Si, L.; Long, K.; Xiao, Z.; Qiu, T.; Chu, P. K. Tunable fluorescence from patterned silver nano-island arrays for sensitive sub-cell imaging. *J. Phys. D: Appl. Phys.* **2013**, *46*, 495302, DOI: 10.1088/0022-3727/46/49/495302

3. Ditlbacher, H.; Krenn, J. R.; Felidj, N.; Lamprecht, B.; Schider, G.; Salerno, M.; Leitner, A.; Aussenegg, F. R. Fluorescence imaging of surface plasmon fields. *Appl. Phys. Lett.* **2002**, *80*, 404– 406, DOI: 10.1063/1.1435410

4. Barnes, W. L.; Dereux, A.; Ebbesen, T. W. Surface plasmon subwavelength optics. *Nature* **2003**, *424*, 824, DOI: 10.1038/nature01937

5. Mabe, T.; Zeng, Z.; Bagra, B.; Ryan, J.; Wei, J. Surface Plasmon Resonance of A Bimetallic Nanostructured Film for Enhanced Optical Sensitivity. *ChemistrySelect* **2018**, *3*, 3018– 3023, DOI: 10.1002/slct.201800576

6. Li, M.; Cushing, S. K.; Wu, N. Plasmon-enhanced optical sensors: a review. *Analyst* **2015**, *140*, 386– 406, DOI: 10.1039/c4an01079e

7. Bauch, M.; Toma, K.; Toma, M.; Zhang, Q.; Dostalek, J. Plasmon-Enhanced Fluorescence Biosensors: a Review. *Plasmonics* **2014**, *9*, 781– 799, DOI: 10.1007/s11468-013-9660-5

8. Homola, J. Surface Plasmon Resonance Sensors for Detection of Chemical and Biological Species. *Chem. Rev.* **2008**, *108*, 462– 493, DOI: 10.1021/cr068107d

9. van den Wildenberg, S. M. J. L.; Prevo, B.; Peterman, E. J. G. A Brief Introduction to Single-Molecule Fluorescence Methods. In *Single Molecule Analysis: Methods and Protocols*; Peterman, E. J. G., Ed.; Springer New York: New York, NY, 2018; pp 93– 113.

10. Fort, E.; Grésillon, S. Surface enhanced fluorescence. *J. Phys. D: Appl. Phys.* **2008**, *41*, 013001, DOI: 10.1088/0022-3727/41/1/013001

11. Li, X.; He, Y.; Que, L. Fluorescence Detection and Imaging of Biomolecules Using the Micropatterned Nanostructured Aluminum Oxide. *Langmuir* **2013**, *29*, 2439– 2445, DOI: 10.1021/la304833u

12. Fu, Y.; Zhang, J.; Lakowicz, J. R. Largely Enhanced Single-Molecule Fluorescence in Plasmonic Nanogaps Formed by Hybrid Silver Nanostructures. *Langmuir* **2013**, *29*, 2731– 2738, DOI: 10.1021/la3048399

13. Tam, F.; Goodrich, G. P.; Johnson, B. R.; Halas, N. J. Plasmonic Enhancement of Molecular Fluorescence. *Nano Lett.* **2007**, *7*, 496– 501, DOI: 10.1021/nl062901x

14. Pattnaik, P. Surface Plasmon Resonance: Applications in Understanding Receptor-Ligand Interaction. *Appl. Biochem. Biotechnol.* **2005**, *126*, 079– 092, DOI: 10.1385/abab:126:2:079

15. Homola, J.; Yee, S. S.; Gauglitz, G. Surface plasmon resonance sensors: review. *Sens. Actuators, B* **1999**, *54*, 3– 15, DOI: 10.1016/s0925-4005(98)00321-9

16. Xu, D.-D.; Liu, C.; Li, C.-Y.; Song, C.-Y.; Kang, Y.-F.; Qi, C.-B.; Lin, Y.; Pang, D.-W.; Tang, H.-W. Dual Amplification Fluorescence Assay for Alpha Fetal Protein Utilizing Immunohybridization Chain Reaction and Metal-Enhanced Fluorescence of Carbon Nanodots. *ACS Appl. Mater. Interfaces* **2017**, *9*, 37606– 37614, DOI: 10.1021/acsami.7b11659

17. Zhang, Y.; Zhang, J.; Zhang, J.; Lin, S.; Huang, Y.; Yuan, R.; Liang, X.; Xiang, W. Intense enhancement of yellow luminescent carbon dots coupled with gold nanoparticles toward white LED. *Dyes Pigm.* **2017**, *140*, 122– 130, DOI: 10.1016/j.dyepig.2017.01.043

18. Miao, P.; Han, K.; Tang, Y.; Wang, B.; Lin, T.; Cheng, W. Recent advances in carbon nanodots: synthesis, properties and biomedical applications. *Nanoscale* **2015**, *7*, 1586– 1595, DOI: 10.1039/c4nr05712k

19. Zeng, Z.; Zhang, W.; Arvapalli, D. M.; Bloom, B.; Sheardy, A.; Mabe, T.; Liu, Y.; Ji, Z.; Chevva, H.; Waldeck, D. H.; Wei, J. A fluorescence-electrochemical study of carbon nanodots (CNDs) in bio- and photoelectronic applications and energy gap investigation. *Phys. Chem. Chem. Phys.* **2017**, *19*, 20101– 20109, DOI: 10.1039/c7cp02875j

20. Wang, L.; Zhu, S.-J.; Wang, H.-Y.; Qu, S.-N.; Zhang, Y.-L.; Zhang, J.-H.; Chen, Q.-D.; Xu, H.-L.; Han, W.; Yang, B.; Sun, H.-B. Common Origin of Green Luminescence in Carbon Nanodots and Graphene Quantum Dots. *ACS Nano* **2014**, *8*, 2541– 2547, DOI: 10.1021/nn500368m

21. Hola, K.; Bourlinos, A. B.; Kozak, O.; Berka, K.; Siskova, K. M.; Havrdova, M.; Tucek, J.; Safarova, K.; Otyepka, M.; Giannelis, E. P.; Zboril, R. Photoluminescence effects of graphitic core size and surface functional groups in carbon dots: COO– induced red-shift emission. *Carbon* **2014**, *70*, 279– 286, DOI: 10.1016/j.carbon.2014.01.008

22. Nicoli, F.; Verschueren, D.; Klein, M.; Dekker, C.; Jonsson, M. P. DNA Translocations through Solid-State Plasmonic Nanopores. *Nano Lett.* **2014**, *14*, 6917– 6925, DOI: 10.1021/nl503034j

23. Chen, P.; Chung, M. T.; McHugh, W.; Nidetz, R.; Li, Y.; Fu, J.; Cornell, T. T.; Shanley, T. P.; Kurabayashi, K. Multiplex Serum Cytokine Immunoassay Using Nanoplasmonic Biosensor Microarrays. *ACS Nano* **2015**, *9*, 4173– 4181, DOI: 10.1021/acsnano.5b00396

24. Luo, Z.; Vora, P. M.; Mele, E. J.; Johnson, A. T. C.; Kikkawa, J. M. Photoluminescence and band gap modulation in graphene oxide. *Appl. Phys. Lett.* **2009**, *94*, 111909, DOI: 10.1063/1.3098358

25. Baker, S. N.; Baker, G. A. Luminescent Carbon Nanodots: Emergent Nanolights. *Angew. Chem., Int. Ed.* **2010**, *49*, 6726– 6744, DOI: 10.1002/anie.200906623

26. Cushing, S. K.; Li, M.; Huang, F.; Wu, N. Origin of Strong Excitation Wavelength Dependent Fluorescence of Graphene Oxide. *ACS Nano* **2014**, *8*, 1002– 1013, DOI: 10.1021/nn405843d

27. Zhu, S.; Shao, J.; Song, Y.; Zhao, X.; Du, J.; Wang, L.; Wang, H.; Zhang, K.; Zhang, J.; Yang, B. Investigating the surface state of graphene quantum dots. *Nanoscale* **2015**, *7*, 7927– 7933, DOI: 10.1039/c5nr01178g

28. Li, H.; He, X.; Kang, Z.; Huang, H.; Liu, Y.; Liu, J.; Lian, S.; Tsang, C. H. A.; Yang, X.; Lee, S.-T. Water-Soluble Fluorescent Carbon Quantum Dots and Photocatalyst Design. *Angew. Chem., Int. Ed.* **2010**, *49*, 4430– 4434, DOI: 10.1002/anie.200906154

29. Sun, Y.-P.; Zhou, B.; Lin, Y.; Wang, W.; Fernando, K. A. S.; Pathak, P.; Meziani, M. J.; Harruff, B. A.; Wang, X.; Wang, H.; Luo, P. G.; Yang, H.; Kose, M. E.; Chen, B.; Veca, L. M.; Xie, S.-Y. Quantum-Sized Carbon Dots for Bright and Colorful Photoluminescence. *J. Am. Chem. Soc.* **2006**, *128*, 7756– 7757, DOI: 10.1021/ja062677d

30. Cao, L.; Meziani, M. J.; Sahu, S.; Sun, Y.-P. Photoluminescence Properties of Graphene versus Other Carbon Nanomaterials. *Acc. Chem. Res.* **2013**, *46*, 171– 180, DOI: 10.1021/ar300128j

31. Liu, R.; Wu, D.; Liu, S.; Koynov, K.; Knoll, W.; Li, Q. An Aqueous Route to Multicolor Photoluminescent Carbon Dots Using Silica Spheres as Carriers. *Angew. Chem., Int. Ed.* **2009**, *48*, 4598– 4601, DOI: 10.1002/anie.200900652

32. Zhang, L.; Song, Y.; Fujita, T.; Zhang, Y.; Chen, M.; Wang, T.-H. Large Enhancement of Quantum Dot Fluorescence by Highly Scalable Nanoporous Gold. *Adv. Mater.* **2013**, *26*, 1289– 1294, DOI: 10.1002/adma.201304503

33. Ming, T.; Chen, H.; Jiang, R.; Li, Q.; Wang, J. Plasmon-Controlled Fluorescence: Beyond the Intensity Enhancement. *J. Phys. Chem. Lett.* **2012**, *3*, 191– 202, DOI: 10.1021/jz201392k

34. Nooney, R. I.; Stranik, O.; McDonagh, C.; MacCraith, B. D. Optimization of Plasmonic Enhancement of Fluorescence on Plastic Substrates. *Langmuir* **2008**, *24*, 11261– 11267, DOI: 10.1021/la801631w

35. Guo, D.-Y.; Shan, C.-X.; Liu, K.-K.; Lou, Q.; Shen, D.-Z. Surface plasmon effect of carbon nanodots. *Nanoscale* **2015**, *7*, 18908– 18913, DOI: 10.1039/c5nr05918f

36. Bukasov, R.; Filchakova, O.; Gudun, K.; Bouhrara, M. Strong Surface Enhanced Florescence of Carbon Dot Labeled Bacteria Cells Observed with High Contrast on Gold Film. *J. Fluoresc.* **2018**, *28*, 1– 4, DOI: 10.1007/s10895-017-2194-z

37. Lalanne, P.; Hugonin, J. P.; Rodier, J. C. Theory of Surface Plasmon Generation at Nanoslit Apertures. *Phys. Rev. Lett.* **2005**, *95*, 263902, DOI: 10.1103/physrevlett.95.263902

38. Zeng, Z.; Mendis, M. N.; Waldeck, D. H.; Wei, J. A semi-analytical decomposition analysis of surface plasmon generation and the optimal nanoledge plasmonic device. *RSC Adv.* **2016**, *6*, 17196– 17203, DOI: 10.1039/c6ra01105e

39. Zeng, Z.; Mabe, T.; Zhang, W.; Bagra, B.; Ji, Z.; Yin, Z.; Allado, K.; Wei, J. Plasmon-exciton Coupling in Photosystem I Based Biohybrid Photoelectrochemical Cells. *ACS Appl. Bio Mater.* **2018**, *1*, 802– 807, DOI: 10.1021/acsabm.8b00249

40. Zhang, W.; Zeng, Z.; Wei, J. Electrochemical Study of DPPH Radical Scavenging for Evaluating the Antioxidant Capacity of Carbon Nanodots. *J. Phys. Chem. C* **2017**, *121*, 18635– 18642, DOI: 10.1021/acs.jpcc.7b05353

41. Li, W.; Zhang, Z.; Kong, B.; Feng, S.; Wang, J.; Wang, L.; Yang, J.; Zhang, F.; Wu, P.; Zhao, D. Simple and Green Synthesis of Nitrogen-Doped Photoluminescent Carbonaceous Nanospheres for Bioimaging. *Angew. Chem., Int. Ed.* **2013**, *52*, 8151– 8155, DOI: 10.1002/anie.201303927

42. Zhu, S.; Song, Y.; Zhao, X.; Shao, J.; Zhang, J.; Yang, B. The photoluminescence mechanism in carbon dots (graphene quantum dots, carbon nanodots, and polymer dots): current state and future perspective. *Nano Res.* **2015**, *8*, 355– 381, DOI: 10.1007/s12274-014-0644-3

43. Georgakilas, V.; Perman, J. A.; Tucek, J.; Zboril, R. Broad Family of Carbon Nanoallotropes: Classification, Chemistry, and Applications of Fullerenes, Carbon Dots, Nanotubes, Graphene, Nanodiamonds, and Combined Superstructures. *Chem. Rev.* **2015**, *115*, 4744– 4822, DOI: 10.1021/cr500304f

44. Lalanne, P.; Hugonin, J. P.; Rodier, J. C. Approximate model for surface-plasmon generation at slit apertures. *J. Opt. Soc. Am. A* **2006**, *23*, 1608– 1615, DOI: 10.1364/josaa.23.001608

45. Zeng, Z.; Liu, Y.; Wei, J. Recent advances in surface-enhanced raman spectroscopy (SERS): Finite-difference time-domain (FDTD) method for SERS and sensing applications. *TrAC, Trends Anal. Chem.* **2016**, *75*, 162– 173, DOI: 10.1016/j.trac.2015.06.009

46. Anger, P.; Bharadwaj, P.; Novotny, L. Enhancement and Quenching of Single-Molecule Fluorescence. *Phys. Rev. Lett.* **2006**, *96*, 113002, DOI: 10.1103/physrevlett.96.113002

47. Cao, E.; Lin, W.; Sun, M.; Liang, W.; Song, Y. Exciton-plasmon coupling interactions: from principle to applications. *Nanophotonics* **2018**, *7*, 145, DOI: 10.1515/nanoph-2017-0059

48. Wu, N. Plasmonic metal-semiconductor photocatalysts and photoelectrochemical cells: a review. *Nanoscale* **2018**, *10*, 2679– 2696, DOI: 10.1039/c7nr08487k

49. Zhu, Z.; Yuan, P.; Li, S.; Garai, M.; Hong, M.; Xu, Q.-H. Plasmon-Enhanced Fluorescence in Coupled Nanostructures and Applications in DNA Detection. *ACS Appl. Bio Mater.* **2018**, *1*, 118– 124, DOI: 10.1021/acsabm.8b00032

50. Lakowicz, J. R.; Ray, K.; Chowdhury, M.; Szmacinski, H.; Fu, Y.; Zhang, J.; Nowaczyk, K. Plasmon-controlled fluorescence: a new paradigm in fluorescence spectroscopy. *Analyst* **2008**, *133*, 1308– 1346, DOI: 10.1039/b802918k

51. Cushing, S. K.; Li, J.; Meng, F.; Senty, T. R.; Suri, S.; Zhi, M.; Li, M.; Bristow, A. D.; Wu, N. Photocatalytic Activity Enhanced by Plasmonic Resonant Energy Transfer from Metal to Semiconductor. *J. Am. Chem. Soc.* **2012**, *134*, 15033– 15041, DOI: 10.1021/ja305603t

52. Li, J.; Cushing, S. K.; Meng, F.; Senty, T. R.; Bristow, A. D.; Wu, N. Plasmon-induced resonance energy transfer for solar energy conversion. *Nat. Photonics* **2015**, *9*, 601, DOI: 10.1038/nphoton.2015.142

53. Leenheer, A. J.; Narang, P.; Lewis, N. S.; Atwater, H. A. Solar energy conversion via hot electron internal photoemission in metallic nanostructures: Efficiency estimates. *J. Appl. Phys.* **2014**, *115*, 134301, DOI: 10.1063/1.4870040

54. Cushing, S. K.; Wu, N. Progress and Perspectives of Plasmon-Enhanced Solar Energy Conversion. *J. Phys. Chem. Lett.* **2016**, *7*, 666– 675, DOI: 10.1021/acs.jpclett.5b02393